LIVE CELL IMAGING OF CYTOSKELETON INTERACTIONS AND MEMBRANE TOPOLOGY

Luca Chierico[a,b], Adrian S. Joseph[a,b], Andrew L. Lewis[c] and Giuseppe Battaglia[a,b*]

[a]Department of Chemistry, [b]The MRC/UCL Centre for Molecular and Medical Virology, University College London, London, United Kingdom.
[c]Biocompatibles UK Ltd., Farnham Business Park, Weydon Lane, Farnham, United Kingdom.

SI Materials and Methods

Reagents

The synthesis of the diblock copolymer $PMPC_{25}$-$PDPA_{70}$, prepared in our laboratories, is described elsewhere[1]. Methanol, trifluoroacetic acid (TFA), *Sepharose 4B, penicillin, streptomycin, amphotericin B, L-glutamine, CK-869 (Arp2/3 inhibitor),* Phalloidin-ATTO647 (ACTIN), 3-(4,5-dimethylthiazol- 2-yl)-2,5 diphenyl tetrazolium bromide (MTT) and Trypsin-EDTA solution 0.25% *were all purchased from Sigma-Aldrich UK (Poole, Dorset, UK). Dulbecco's Modified Eagle Medium (*DMEM), DMEM imaging media, fetal calf serum (FCS), 2-Decanoyl-1-(O-(11-(4,4-Difluoro-5,7-Dimethyl-4-Bora-3a,4a-Diaza-s-Indacene-3-Propionyl)amino)Undecyl)-sn-Glycero-3-Phosphocholine (BODIPY®phosphocholine - PC), 1-Hexadecanoyl-2-(1-Pyrenedecanoyl)-sn-Glycero-3-Phosphocholine (β-Py-C10-HPC), 22-(N-(7-Nitrobenz-2-Oxa-1,3-Diazol-4-yl) Amino)-23,24-Bisnor-5-Cholen-3β-Ol (NBD-Cholesterol - CHOL), N-((4-(4,4-difluoro-5-(2-thienyl)-4-bora-3a, 4a-diaza-s-indacene-3-yl)phenoxy)acetyl)sphingosine (BODIPY®TR Sphingosine - S) and Lipofectamine LTX were purchased from Invitrogen (UK). Phosphate Buffer Saline (PBS) was bought from Oxoid Ltd. Chloroform and sodium hydroxide was obtained from Fisher Scientific (UK) and hydrochloric acid from BDH AnalaR (UK). 1,2-dipalmitoyl-sn-glycero-3-phosphoethanolamine-N-(lissamine rhodamine B sulfonyl) - PE) and the TopFluor® *phosphatidylinositol 4,5-bisphosphate* (TopFluor PIP2 - PIP2) were bought from Avanti Polar Lipids Inc. (USA). The Mouse embryonic fibroblast cell line (NIH-3T3) were obtained from ATCC® the global bio-resource center. The glass bottom petri dishes were bought from IBIDI® (Thistle Scientific LTD, UK). The plasmid CFP-PLCdelta-PH was obtained from addgene (USA). All the imaging analyses were performed with a Leica TCS SP8 confocal laser microscope.

Polymersomes preparation and cargo encapsulation

All the polymersomes samples used in the study were prepared combining $1x10^{-3}$ moles of copolymer $PMPC_{25}$-$PDPA_{70}$ with $5x10^{-5}$ moles of amphiphilic/hydrophilic cargo. The two compounds, the diblock copolymer and the respective cargo, were solubilized and mixed together in a solution of 2:1 chloroform:methanol in a glass vial. After that, a film was formed by placing the vial containing the solution in a vacuum desiccator overnight, until a complete solvent evaporation. Finally, the vials were rehydrated by adding 2 ml of PBS at pH 7.4. The polymersomes formation was achieved placing the solution in stirring condition for 20 days. At this point, the polymersomes sample was purified from any non-encapsulated material using a size exclusion chromatography based on Sepharose 4B. Polymersomes were then characterized with Dynamic Light Scattering (DLS), and Transmission Electron Microscopy (TEM) analyses. The calculation of total amount of encapsulated cargo, into a single polymersome vesicle (L_{EE} = Loading encapsulation efficiency), was performed with the a Reverse Phase High Performance Liquid Chromatography (RP-HPLC) analysis, with a multistep water/methanol gradient in 5% of TFA [2]. As shown in Figure S1, all the results are indicating a great average in terms of L_{EE} for all the cargoes encapsulated. In particular, the results confirmed an average loading efficiency value (number of molecules encapsulated per

single polymersome) between 1185 (CHOL) to 3363 (PC) regarding the phospholipidic cargoes with an exception represented by the PIP2. For this latter molecule, in fact, the obtained average L_{EE} was 90 molecules per polymersome. On the other side, the L_{EE} of ACTIN (that is the only hydrophilic molecule used in the study) was found to be 40 peptide molecules per single polymersome. The difference in the encapsulation efficiency is due to the physicochemical properties of the molecules, as well as to their physical distribution within the polymersomes. The physicochemical proprieties of an amphiphilic molecule, such as phospholipids, allow in fact their distribution into the synthetic polymer membrane [3]. On the other hand, hydrophilic molecules, such as Phalloidin, are confined in the polymersomes lumen space [4]. The real space available is, in this case, negligible. Hence, it is also necessary to take into account the actual volume occupied by each single molecule. Taken together, all these factors contribute to the smaller L_{EE} value achieved for ACTIN.

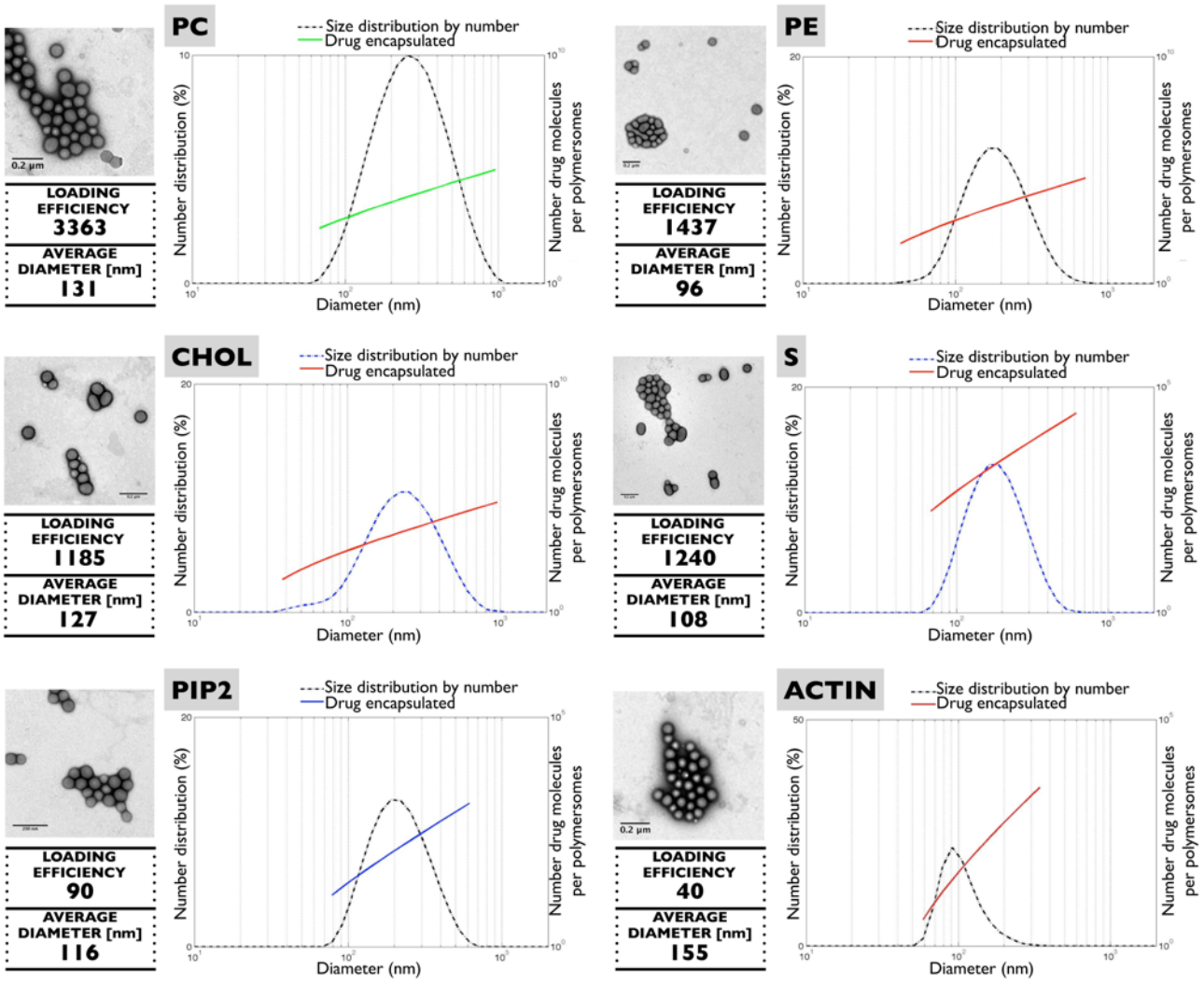

Figure S1. The DLS and TEM characterization analyses confirmed a stable polymersome formation. The knowledge of both the particle diameter and the formation efficiency, combined with RP-HPLC analysis, allowed the L_{EE} value calculations.

Polymersomes as an efficient and biocompatible delivery vector for amphiphilic and hydrophilic molecules

In this study, the possibility to use polymersome as synthetic vector (to achieve a stable delivery of both amphiphilic and hydrophilic molecules in live cells) is demonstrated. Five different amphiphilic compounds were tested: PC, PE, CHOL, S, PIP2 and ACTIN (the only hydrophilic molecules). A confocal laser scanning analysis was used to test their specific distribution within the cell. For all the formulations, cell viability was tested in NIH-3T3 cell line. In particular, cells were seeded in a 24-well plate, at a density of 3 x 10^4 cells per well, and grown for 48 hours in complete DMEM medium. After this, cells were divided in seven groups, and treated for 24 h with fresh medium containing 10% volume of PBS (negative control), and six different polymersomes formulations: PC, PE, CHOL, S, PIP2 and ACTIN, all at 1 mg/ml final polymersomes concentration. Cell viability was assessed using the MTT assay. Treated and control cells were washed three times with PBS and then incubated in MTT solution (0.5 mg mL^{-1} MTT in PBS, 1 mL per well of 24-well) for 1 h at 37˚C / 95% air / 5% CO_2. Intracellular metabolic activity reduces MTT to a purple formazan salt. Subsequently, the solution was eliminated and the insoluble formazan product was solubilized by adding isopropanol (0.5 mL per well of 24-well plate) and incubated for 5 min. The results were measured using a plate reader spectrophotometer with optical density at 570 nm (Dynex Technologies, MRX II). Figure S2A-B demonstrates the effective delivery and the MTT results of all the six different formulations. Because of the interactions between Phal loidin and actin monomers, and the Phalloidin mechanism of action that can interfere with F-actin de-polymerisation, it was also necessary to asses, for the ACTIN probe, the cell motility after treatment. To study this, a control experiment was performed, where cell motility was evaluated (through a low magnification microscope analysis) in an interval of 32 h after polymersomes incubation and control treatment. Cells were seeded at a density of 2 x 10^3 cells per well, and grown in a cell culture dish with an appropriate silicon insert defining a gap of 500 μm. The two cell populations (NIH-3T3 cell line) were treated with PBS (10% in volume as a negative control) and ACTIN polymersomes formulation, for 24 h, respectively. Upon reaching the total confluence, the silicone support was removed to allow cell spreading in between the gap. Then, several low magnification (10X) DIC (Differential interference contrast) confocal analysis, at consecutive time points, were carried out, while the free area left by the cells was analyzed by imageJ software. Specifically, the free area left by the spreading cells was evaluated during time, comparing the two treatments. As shown by Figure S2D, there are no differences in cell motility between the two experiments. This confirms that the ACTIN probe have no detectable effects on F-actin polymerization and cell motility. Previous works showed that, at high concentration, Phalloidin can hinder F-actin de-polymerization by stabilizing the protein in its polymerized form [5], resulting in limited cell motility. This experiment show that the Phalloidin delivered concentration (by the polymersomes) is enough to stain the actin filaments without interfering/perturbing the polymerization/de-polymerization cycles. These data were also confirmed by an additional experiment, were the ACTIN probe was co-delivered with the PIP2 (Figure S3). This case enabled to follow, in real time, the cell division process in living cells. In particular, NIH-3T3 cells were first cultured in complete DMEM medium at a density of 1 x 10^4 cell/well for 24 h of incubation time. Then, cells were treated with fresh medium containing PIP2 and ACTIN, both at 1 mg/ml final polymersomes concentration. After 24 h of incubation, cells were rinsed with PBS (three washing steps) and incubated with fresh imaging medium. After this, confocal laser scanning microscopy analyses were carried out on live cells, by applying the same laser setting as previously described.

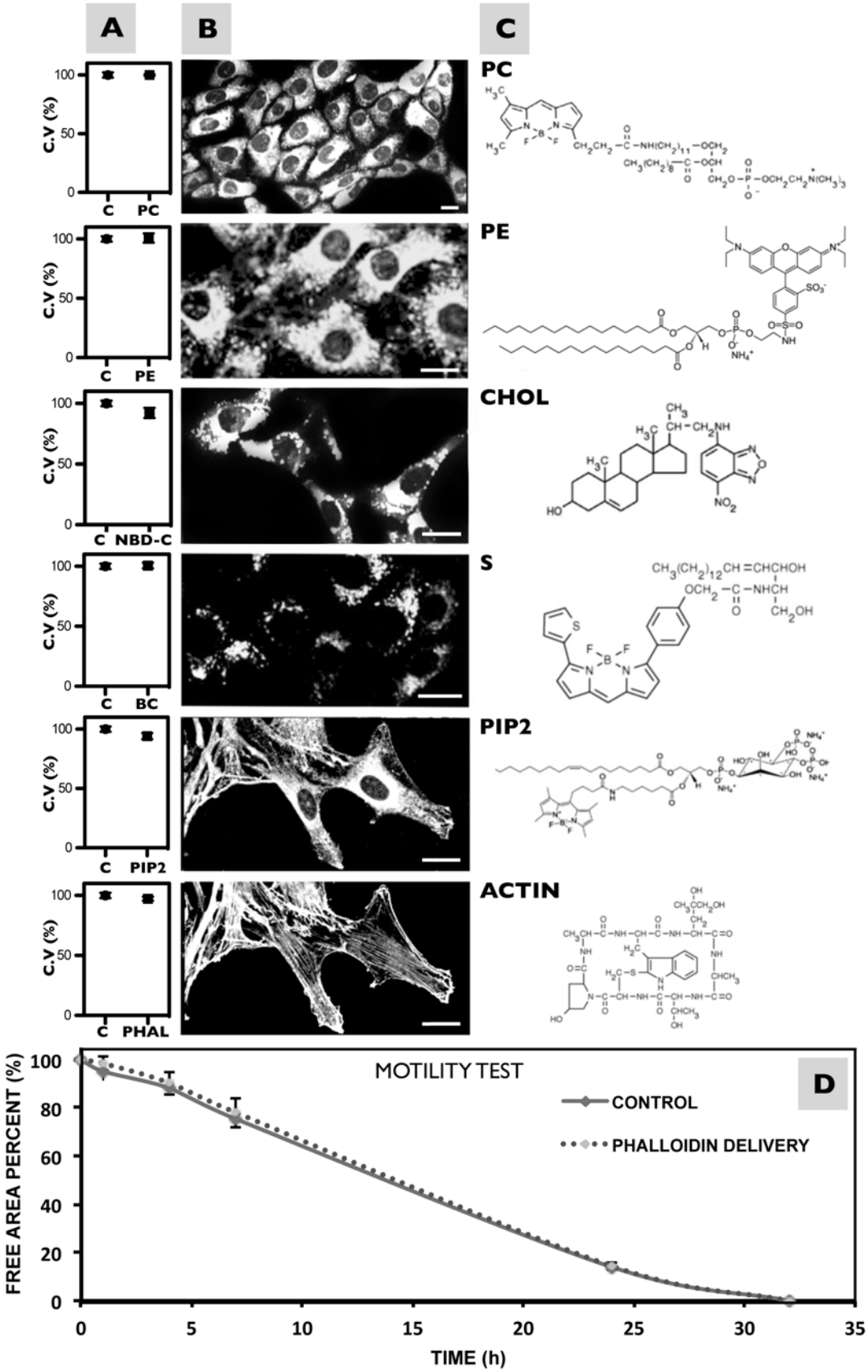

Figure S2. The cell viability percentage (C.V% - A) was calculated per single probe, with respect to the control cells (incubated with PBS). As shown in the table A, all the formulations were non toxic, with a C.V % never below 90%. B) and C) are the live cell confocal investigations and the chemical formula, respectively, of all the probes used, namely PC, RhB-DHPE, CHOL, S, PIP2 and ACTIN. For the ACTIN plymersomes delivered sample, the cell motility after treatment was also characterized. This was done with a motility assay, comparing ACTIN treated cells with a control, represented by cells treated with 10% PBS in medium. The graph in D represents the free area percentage (%) left by spreading cells at different time points. This result was achieved using a cells scratch assay, while the free area was calculated through imageJ software. Scale bar: 20 µm.

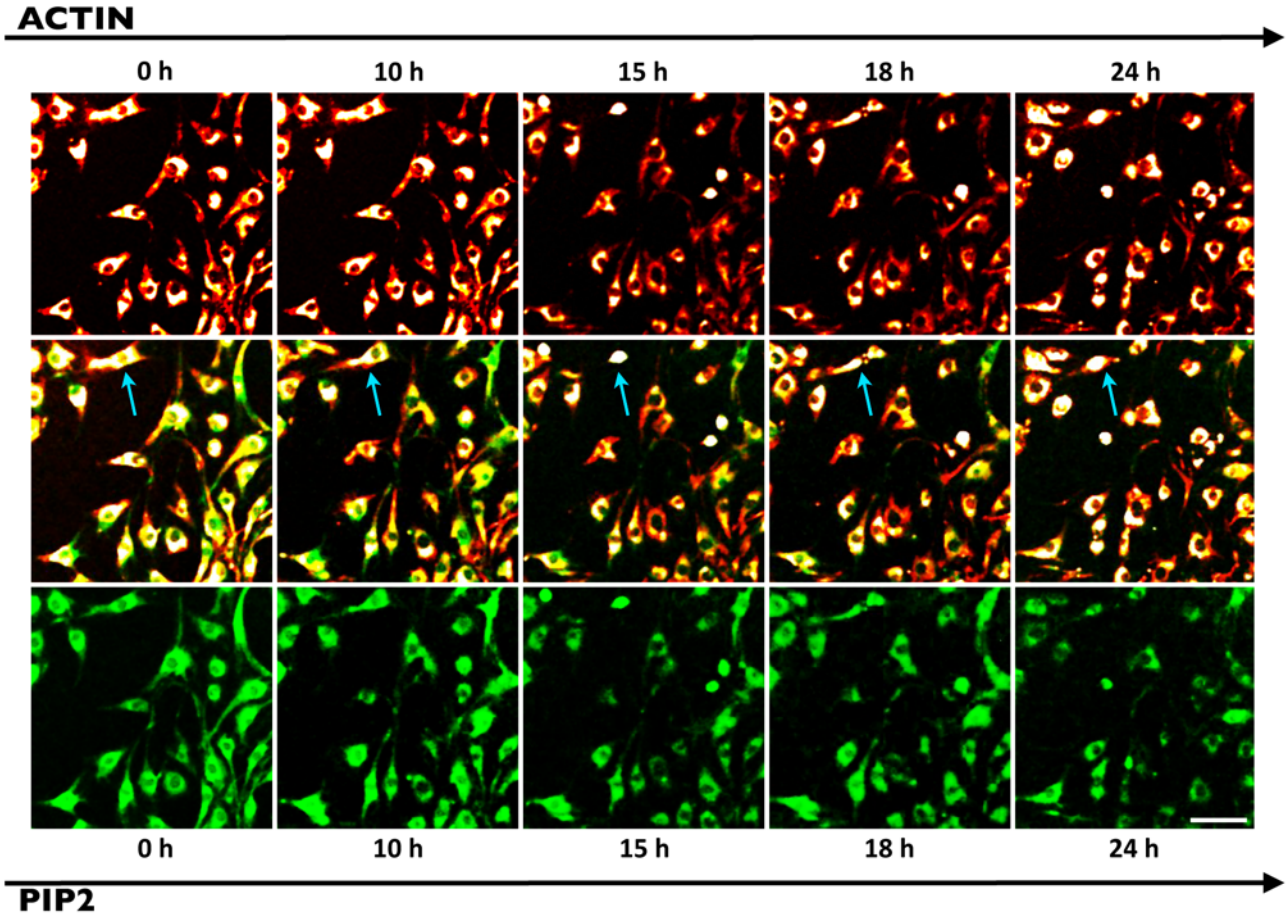

Figure S3. PIP2 and ACTIN polymersome delivery in NIH-3T3 cell line. The live cell confocal analysis was carried out for 24 h. Scale bar: 100 µm.

Cytoskeleton and inositol interactions

To verify the strong interaction between actin structure and inositol, a specific experiment was setup. NIH-3T3 cells were incubated for 24 h with two polymersomes formulations (same concentration as previously reported) carrying PIP2 and ACTIN probes. Then, 10 uM of Arp 2/3 inhibitor (CK-869) was added [6]. The negative control was treated with 10% PBS. After this, cells were analyzed with confocal laser scanning microscope, using the same settings reported in the previous paragraph. As shown in Figure S4, a relevant signal for both the probes was detected, in agreement with the previous data. Also for the Arp2/3 treated cells (CK-869), a relevant colocalization between the PIP2 and ACTIN was found, demonstrating again significant interactions between the two molecules. All these data were further corroborates by an overlap quantification, performed with a MATLAB® software. The results of this analysis, showed in Figure S4, indicates an average in the overlap percentage value higher than 80% in both the cell centre and edge. To further clarify this particular interaction, another colocalization experiment was performed. In this case, the possible cooperation between PE and the F-actin was investigated. PE was used as a prove of concept, because there are not significant evidences demonstrating a specific localization/interaction between this phospholipid and the actin structures [7]. In our experiment, three probes were simultaneously delivered: ACTIN, PIP2 and PE, with experimental conditions as previously reported for PE imaging, $\lambda_{ex}/\lambda_{em}$ of 540 nm / 625 nm were used. The results, in Figure S5, confirmed an average-overlap signal value lower than 45% in the central area, and close to 30% at the periphery, for untreated cells (Figure S5A). Upon treatment with CK-869, a significant

increase in the overlap value was identified in the central area (~65%). This result is probably due to an apoptotic process induced by the drug action, and to an intracellular vesicular accumulation of all the delivered probes. On other hand, the calculated overlap between ACTIN and PIP2 is similar to the value detected in the previous experiment (Figure S4). Taken together, all these findings demonstrated the high efficiency of polymersomes for the co-delivery of several different cargoes, as well as they confirm the ability of polymersomes to effectively integrated the desired molecules within the complex cell machinery, in a precise manner.

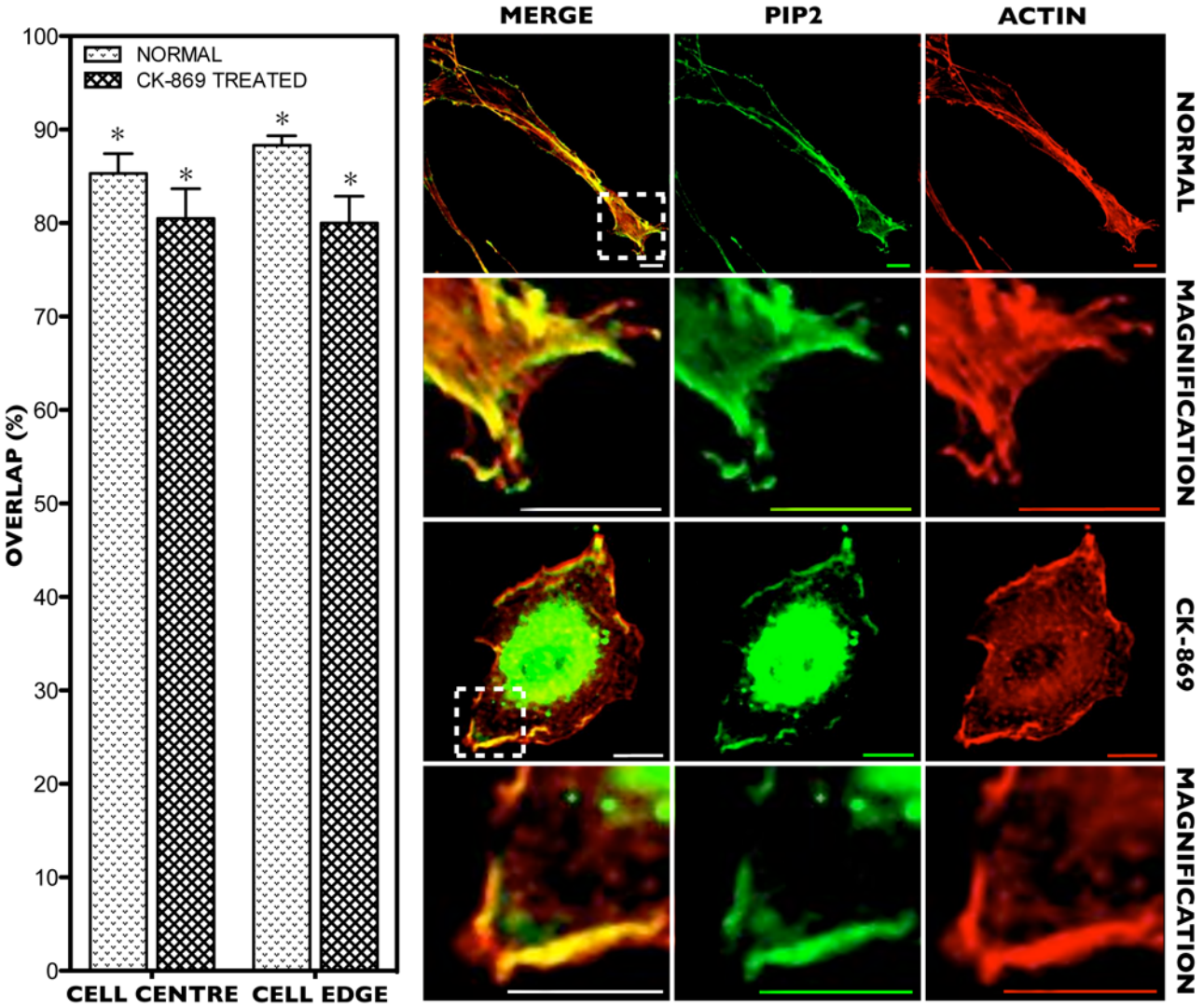

Figure S4. Polymersome delivery of ACTIN and PIP2 in NIH-3T3 cells. The overlap fluorescence value percentage (table above) between PIP2 and ACTIN was similar between untreated and Arp 2/3 inhibitor (CK-869) treated cells. This to show the ACTIN and PIP2 intrinsic and specific interaction. The figures and the table above show a great overlap between the two molecules (~85%), indicating a specific accumulations of both signals (PIP2 and ACTIN) in the two conditions (untreated and CK-869 treated cells), regarding the two analyzed areas (the cell centre and cell edge). (*t-test, p-value > 0.05) No statistical differences between three independent experiments. Scale bar: 15 µm.

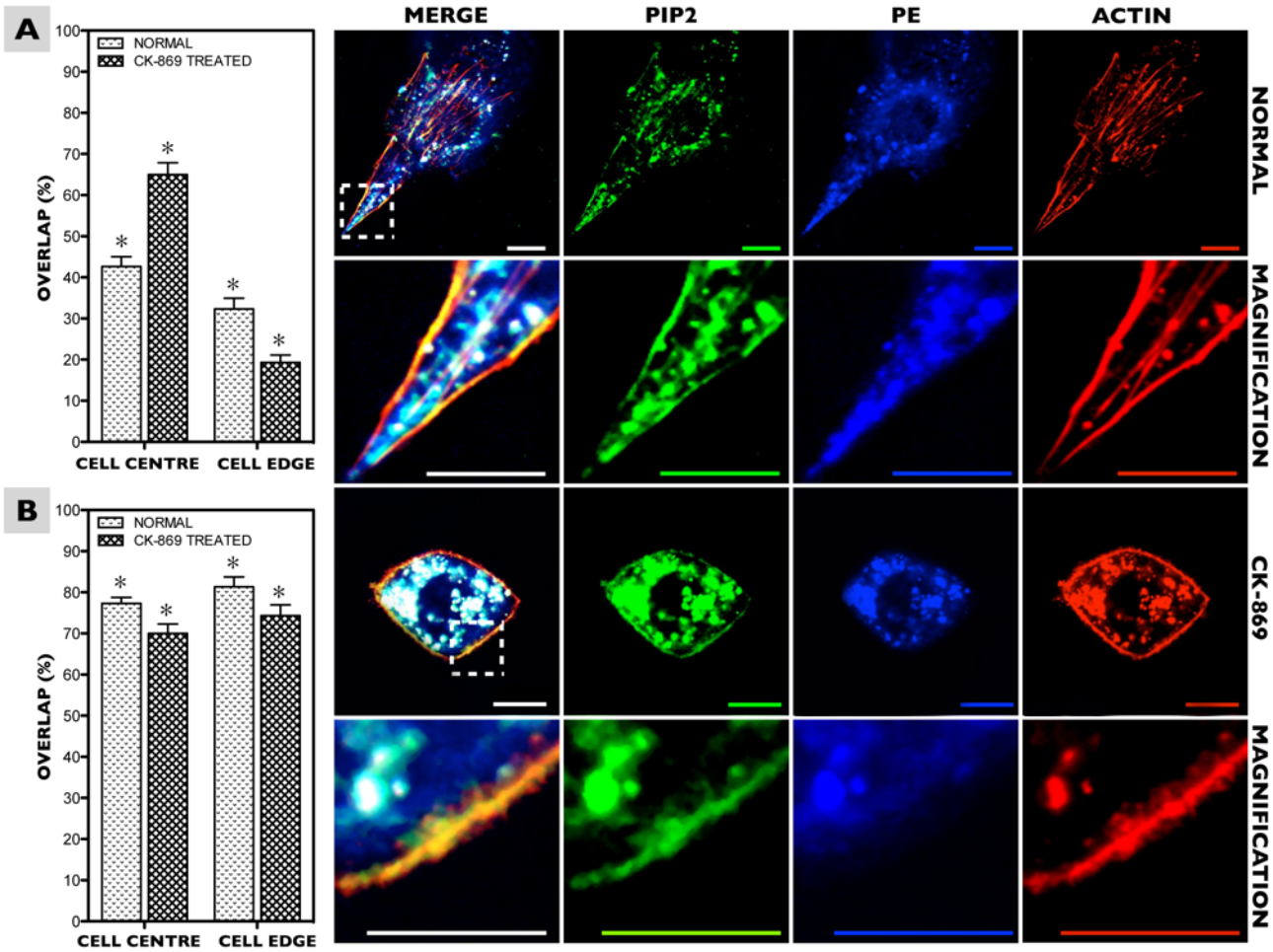

Figure S5. Polymersome delivery of ACTIN and PIP2 in NIH-3T3 cells. The figures are showing the poor and unspecific interaction between the F-actin network and the PE, in two investigated areas (cell centre and cell edge). These results are further confirmed by an overlap calculation represented by the A. The overlap-increased value at the cell centre, upon CK-869 treatment, is probably due to a drug apoptotic induction and consequent cytoplasmic probes accumulations. In B, also in this case, it is shown the high overlap value percentage, between PIP2 and ACTIN, for both untreated and CK-869 treated cells. (*t-test, p-value > 0.05) No statistical differences between three independent experiments. Scale bar: 15 µm.

PIP2 and CFP-PLCd-PH colocalization study

To evaluate the natural PIP2 distribution at the cell membrane level, we performed a colocalization study between our PIP2 delivered probe and the CFP-PLCdelta-PH.
As reported in other works, this construct codify for the pleckstrin homology (PH) domains of protein lipase C delta, that specifically interact with PIP2 [8,9]. The used pDNA presented also the nucleotidic sequence to express the cyan fluorescent protein (CFP) that can be visualized by means of confocal laser scanning microscopy with the following parameters: $\lambda_{ex}/\lambda_{em}$ of 350 nm / 470 nm.
As previously described, initially the NIH-3T3 were seeded in glass bottom dishes (35 mm diameter) with a density of 8 x 10^3 cells/well, and incubated for 24 h in complete DMEM medium.
Subsequently, the cells were transfected with the chosen pDNA, using Lipofectamine LTX transfection reagent with a final pDNA concentration of 3.7 µg/ml. At this point cells were incubate in DMEM medium for 24 h. After that, they were treated as previously described with the PIP2 formulations and then analyzed in a confocal imaging experiment. The results obtained are reported below.

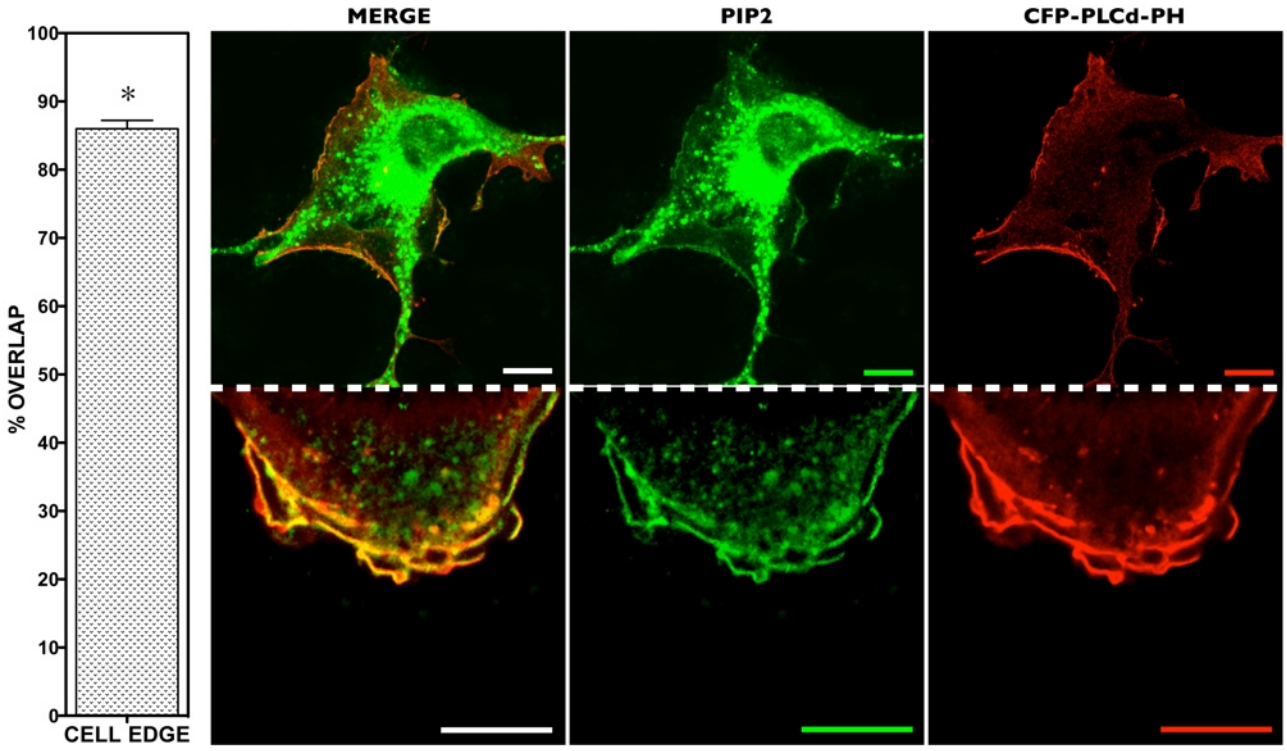

Figure S6. PIP2 and CFP-PLCdelta-PH confocal analysis in NIH-3T3 cell line. The confocal overlap experiment between these two compounds, confirmed the natural membrane distribution of the labeled PIP2 derivate used in the study. (*t-test, p-value > 0.05) No statistical differences between three independent experiments. Scale bar: 10 µm.

Probe intracellular distribution: dye dependence study

To demonstrate that the physicochemical properties of phospholipids and their membrane distributions were not affected by the presence of a dye, another control experiment was carried out. In this case, two differently labelled phosphocholine were encapsulated into the polymersome vector, namely BODIPY®PC and the β-Py-C10-HPC. These two molecules have a similar structure, and differ for the presence of the different dye, that are the 4-difluoro-4-bora-3a,4a-diaza-s-indacene and the pyrene respectively. The aim of this experiment was, hence, the evaluations of any relevant difference in term of membrane distributions, between the probes. The cells were then treated with the two samples (with the same method as the previous probe treatment), and subsequently analyzed through a confocal imaging experiment with $\lambda_{ex}/\lambda_{em}$ of 490 nm / 525 nm for the PC and 345 nm / 380 nm for the β-Py-C10-HPC. The results strongly indicate a solid overlap between the two channels (Figure S7), demonstrating that the dye does not affect itself the distribution of the phospholipids within the membrane.

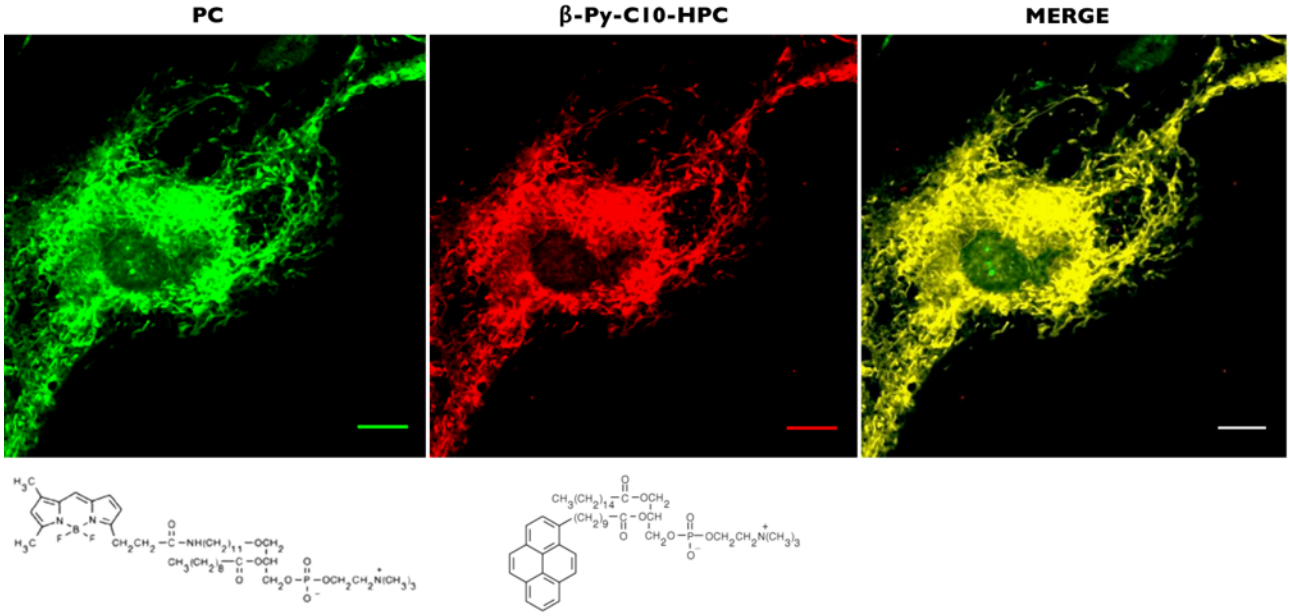

Figure S7. PC and β-Py-C10-HPC pollymersome delivery in NIH-3T3 cell line. The confocal overlap experiment between these two compounds, which differ for the dye molecule, confirmed that the labeled lipid derivates used in the study are not influenced in the membrane distribution by the dye proprieties. Scale bar: 10 µm.

Probe intracellular distribution: concentration dependence study

Lipid clustering may occur if the lipid concentration is significantly altered by exogenous delivery. To exclude such a possibility, we estimated the amount of lipid delivered with respect to the endogenous level using the following equation:

$$\text{TOTAL ADDED PER CELL (\%)} = \frac{\text{TOTAL µg PER TREATMENT}}{\text{CELL VOLUME (L)} * \text{CELLS NUMBER} * \text{MW LIPID} * \text{EFFECTIVE CONC. PER CELL (µM)}} * 100$$

Assuming that all the lipid probe is delivered, and using the endogenous lipid concentration value available in literature, we can calculate the ratio between our delivered probe and the endogenous lipid population [7,10-12].
The results are reported in the table below.

MOLECULE	EFFECTIVE CONC. PER CELL (µM)	TOTAL µg PER TREATMENT	CELLS NUMBER	CELL VOLUME (L)	TOTAL ADDED µM PER CELL	TOTAL ADDED PER CELL (%)
PC	300	0.00016	16000	4.19E-12	2.79	0.93
PE	250	0.0002	16000	4.19E-12	2.32	0.92
CHOL	300	0.000064	16000	4.19E-12	1.93	0.64
S	250	0.00009	16000	4.19E-12	1.90	0.76
PIP2 (A)	10	0.000008	160000	4.19E-12	0.0096	0.096
PIP2 (B)	10	0.000008	16000	4.19E-12	0.09	0.96

Table S1. Data resulting from the ratio between our delivered probes and the endogenous cell lipid composition. The reported results indicate an average contribution of the total concentration per singular lipid species lower than 1%.

The resulting average lipid increment is between 0.096% PIP2(A) (relative to cells treated with PIP2 during the cell adhesion and spreading process (Figure 1)) and 0.96% PIP2(B) (value relative to the cytoskeleton and inositol interaction experiments (FigureS4-5)). We can thus assume that such a small increment should cause no effect on the cell lipid homeostasis and hence our probes can be used to map out the different lipid compositions.
Moreover, to strongly support the observations of a natural membrane distribution of delivered probes, and in particular the PIP2 specific cluster formation alongside F-Actin during cellular adhesions process (Figure1), a Z-stack cellular reconstruction of Figure1C is herein reported.

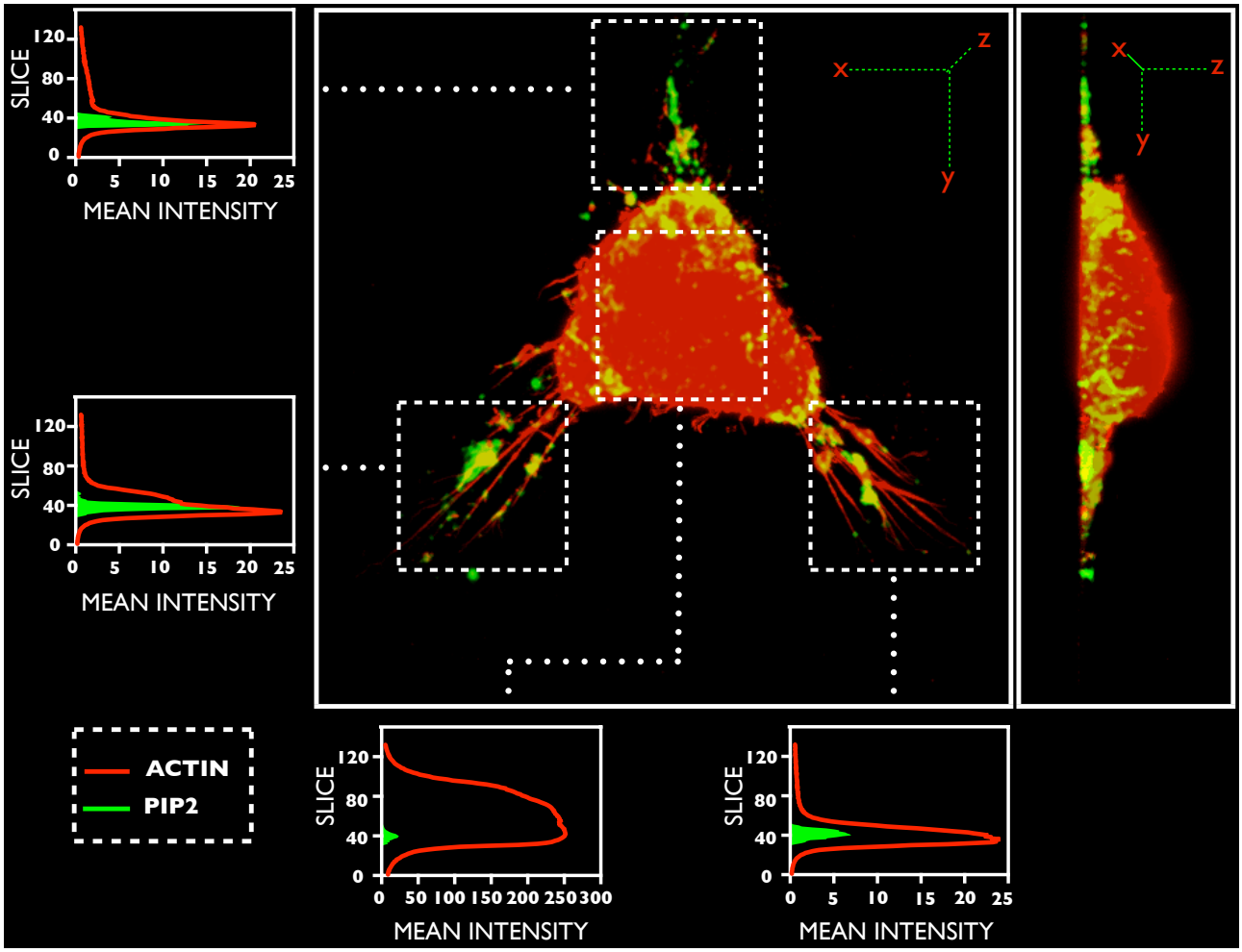

Figure S8. Z-stack cell reconstruction of PIP2 and ACTIN distribution. The latter has also been studied through a Z-stack versus mean intensity graphical reconstruction in four different areas.

As shown in Figure S8, the PIP2 domains are specifically distributed at the cellular bottom level. Furthermore, the Z-stack versus mean intensity graphical reconstruction, considered for four different cell areas, confirmed this observation.

In fact, from this analysis, it is possible to notice that the PIP2 clusters are not just present at the bottom of the cell, but they are particularly accumulated at the cellular protrusions (FigureS8, areas 1,3,4), alongside the F-actin network. On the other hand, there is no evident PIP2 cluster formation at the cellular top membrane level (FigureS8, area 2).

This is again supporting the PIP2 specific membrane localization and interplay with F-actin network during a dynamic process such as cell adhesion.

To further verify the natural distribution of our polymersome-delivered probes, we investigated the sub-cellular localization of another lipid used in this study, namely PC.

This phospholipids is well establish as dominant constituent of the endoplasmic reticulum (ER) membrane [7]. For this reason the evaluation of this cell membrane compound after its polymersome-mediated intracellular delivery, can be adopted as a further validation regarding the natural probes distributions at the cell membrane level of our probes.

For this experiment, NIH-3T3 cells were incubated as previously described in DMEM, containing 1 mg/ml of polymersomes-PC, and then investigated by confocal analysis. Figure S9 shows the intracellular delivery of PC. The accumulation of this probe was found to particularly occur in a defined micro-tubular network, which could be represented by the cell endoplasmic reticulum (ER).

In particular, three specific areas of the cell were analyzed in detail to better evaluate the PC intracellular accumulations. The inset 1 of Figure S9 (describing the cell nucleus area) displays a great accumulation of the probe. This can be related to the abundant presence, in this region, of the two rich lipid membrane compartments cell nucleus and rough endoplasmic reticulum, which may promote the PC accumulations in this specific sub-cellular area. The second magnified inset shows the possible localization of PC probe within the smooth endoplasmic reticulum (Figure S9A), where PC was found to accumulate with higher efficiency. The third analyzed inset (Figure S9A - area number three) is the study of PC distributions at the cellular edge, where the ER network is reduced compared to the plasmatic area. In this case, the signal intensity is considerably lower, probably because of the broad distribution of the delivered probe in the plasma membrane. To confirm these observations, a co-staining experiment with a specific E.R-Tracker™ was performed. Cells were first cultured in DMEM for 24 h in a glass bottom dish, with a density of 4 x 10^3 cells. Then, cells were incubated with the PC-polymersomes formulation as previously described. After this step, cells were rinsed three times with PBS and incubated fresh DMEM containing 100 nM of E.R-Tracker™. After 10 minutes of treatment, cells were washed three times with PBS and then analyzed with a confocal microscope in imaging medium, with $\lambda_{ex}/\lambda_{em}$ of 350 nm / 470 nm to detect the E.R-Tracker™ signal, and $\lambda_{ex}/\lambda_{em}$ of 490 nm / 525 nm for the PC. Figure S9B shows the results of this analysis. Interestingly, the distribution of PC and E.R-Tracker™ is almost identical (with an overlap average value of 94%). This further confirms the natural membrane distribution of the delivered PC, which for this lipid corresponds with the observed accumulation at the E.R level. In addition, the E.R-Tracker™ and the polymersomes-PC toxicity to cells was evaluated with an MTT assay. In particular, NIH 3T3 cells were incubated with 100 nM of E.R-Tracker™ for 30 minutes, and with 1 mg/ml of the polymersomes-PC probe for 24 h, while 10% of PBS was used as negative control. The results highlight a significant E.R-Tracker™-related toxicity (around 50%), while PC did not have metabolic effects on cells (Figure S10A), thus confirming the possibility to exploit the polymersomes-PC as a stable and biocompatible E.R marker for biological studies in live cell imaging.

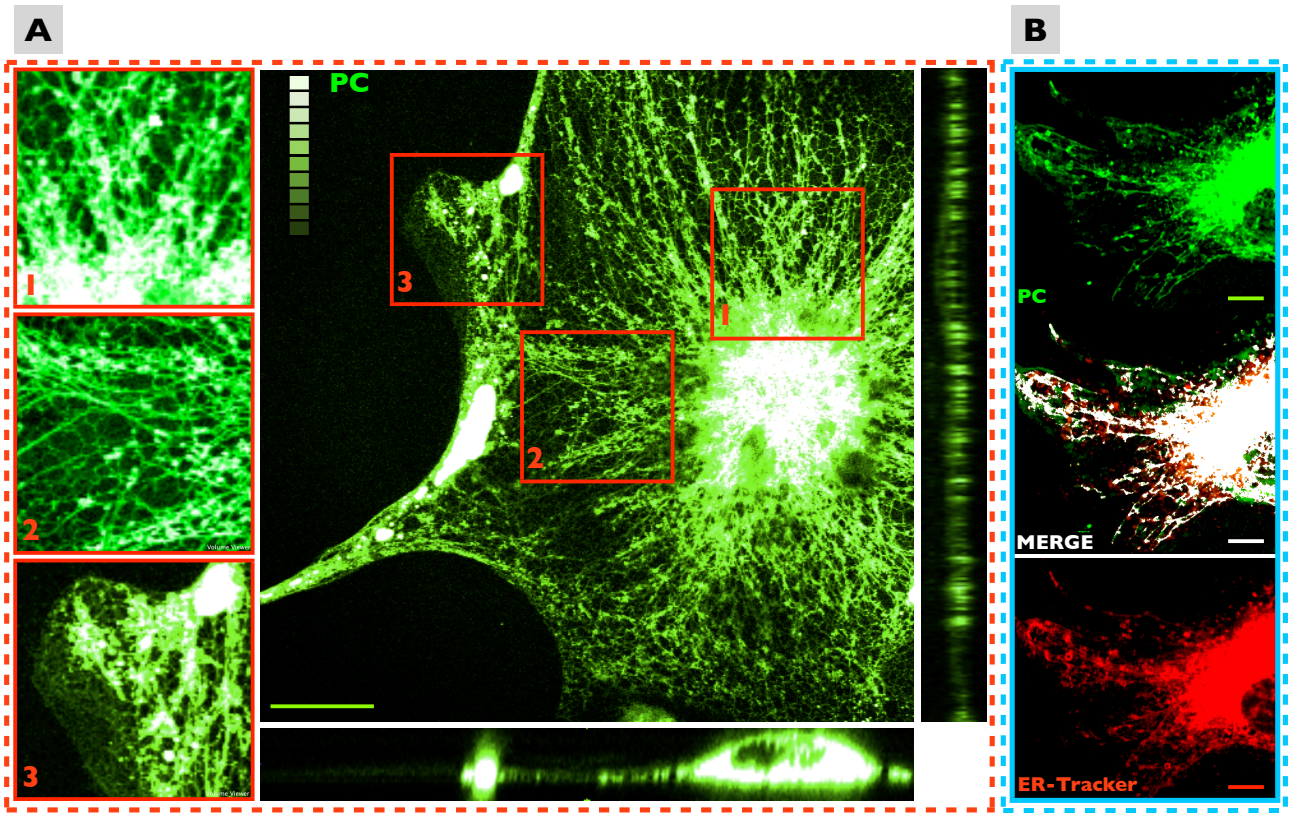

Figure S9. (A) Live cell confocal analysis of PC, delivered by polymersome in NIH-3T3 cell line. (B) Colocalization experiment in live cell between PC and ER-Tracker™. The results show an average overlap value of ~94%, indicating that most part of delivered PC is first stored in the E.R compartment. Scale bar: 20 µm.

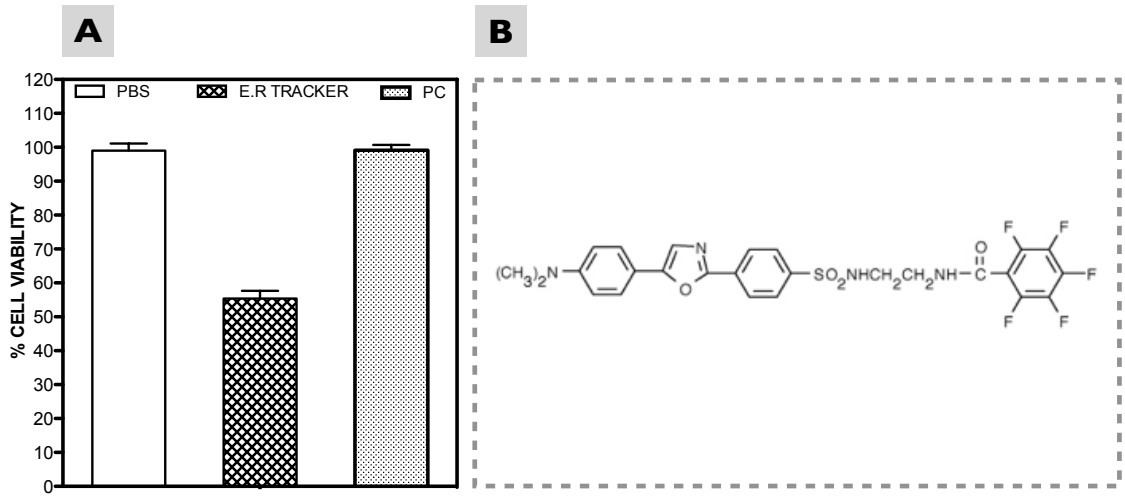

Figure S10. (A) MTT of cell treated with PBS (negative control), E.R-Tracker™ and PC. No toxicity was reveled for PC and PBS, while the E.R-Tracker™ displayed a significant toxicity (~55%). (B) E.R-Tracker™ molecular structure.

MATLAB® code for the colocalization analysis

Sometimes it is useful to separate the contribution of each channel to the colocalization, so to quantify how much of one channel overlaps with the other and vice versa. This is done using the Manders' coefficients [13], splitting r_o into its components:

$$k_1 = \frac{\sum_{i=1}^{n}(R_i G_i)}{\sqrt{\sum_{i=1}^{n}(R_i)^2}} \quad (3)$$

and

$$k_2 = \frac{\sum_{i=1}^{n}(R_i G_i)}{\sqrt{\sum_{i=1}^{n}(G_i)^2}} \quad (4)$$

Because k_1 and k_2 are highly affected by the relative intensity of the channels, the Manders' coefficients are usually calculated only for the colocalized pixels of each separate channel:

$$M_1 = \frac{\sum_{i=1}^{n}(R_{i,coloc})}{\sqrt{\sum_{i=1}^{n}(R_i)^2}} \quad (5)$$

and

$$M_2 = \frac{\sum_{i=1}^{n}(G_{i,coloc})}{\sqrt{\sum_{i=1}^{n}(G_i)^2}} \quad (6)$$

In addition to that, the script provides the possibility to segment the pictures. This was introduced to be able to focus on specific regions of interest of the cells.
In this sense a specific code was developed.
First the code let the user choose the folder were the 8-bit tiff images to be analyzed are stored.
It then build up a database containing all the images and their modification.

```
clear all

 dirname=uigetdir('Choose a directory');

 listing=dir(dirname);
 silis=size(listing);
 silis=silis(1,1);
 silisb=silis+1;
 files=0;
 l=1;
 for i=1:silis
     if listing(i,1).isdir==0
         listing(i,1).name
         ttt=input('Analyse this file? y=1, n=0 ');
         if ttt==1
         files=files+1;
         inde(l,1)=i;
         l=l+1;
         end
     end
 end

for rep=1:files
data{rep,1}=listing(inde(rep,1),1).name;

data{rep,2}=imread(fullfile(dirname,listing(inde(rep,1
    ,1).name));
data{rep,8}=double(data{rep,2});
data{rep,3}=data{rep,8};
data{rep,7}=data{rep,2};
end


sis=size(data);
sis=sis(1,1);
tot=2*sis;
index=1;
```

This second part of the code allow for manual segmentation. Once the user identifies the reference channel MATLAB® will allow to select a region of interest and it will apply it to the other channel.

```
dec0=input('Segment? (N=0, Y=1) ');
if dec0==1
    rrr=input('which image of the couple is the reference
       ? ');
    dec3=input('do you want to select areas to exclude or
        to calculate? exclude=1, calculate=2 ');
for i=rrr:2:sis
    dec2=0;
    while dec2==0

        bw=roipoly(data{i,7});
    if dec3==2
        f=find(bw==0);
    else
        f=find(bw==1);
    end
    data{i,3}(f)=0;
    l=i+1;
    data{l,3}(f)=0;
    close(gcf);
    data{i,7}(f)=0;
    imshow(data{i,7});
    dec2=input('happy? (N=0, Y=1) ');
    close(gcf);
    end
end
close(gcf);
end
```

This block calculates the overlap coefficient as defined by equation 2;

```
display('Calculating overlap coefficient')
for v=1:2:sis
k=size(data{v,3});
k=k(1,1)*k(1,2);
ss=0;
aa=0;
bb=0;
cc=0;
d=v+1;


for i=1:k
    s=data{v,3}(i)*data{d,3}(i);
    ss=ss+s;

    a=(data{v,3}(i)^2);
    aa=aa+a;
    b=(data{d,3}(i)^2);
    bb=bb+b;
end
    cc=aa*bb;
    data{v,5}=ss/sqrt(cc);
    data{d,5}=data{v,5};
g=index*100/tot;
an1=num2str(g);
middle1='%';
Progress=[an1,middle1]
index=index+1;
end
```

This block calculates the Manders' coefficients as defined by equations 5 and 6;

```
display('Starting calculation of M1 coefficients')
for v=1:2:sis
k=size(data{v,3});
k=k(1,1)*k(1,2);
ss=0;
d=v+1;
for i=1:k
    if data{d,3}(i)~=0
    s=data{v,3}(i);
    else
        s=0;
    end
    ss=ss+s;
end
data{v,4}=ss/sum(data{v,3}(:));
g=index*100/tot;
an1=num2str(g);
middle1='%';
```

```
Progress=[an1,middle1]
index=index+1;

end


display('Starting calculation of M2 coefficients')
for v=1:2:sis
k=size(data{v,3});
k=k(1,1)*k(1,2);
ss=0;
d=v+1;
for i=1:k
    if data{v,3}(i)~=0
    s=data{d,3}(i);
    else
        s=0;
    end
    ss=ss+s;
end
data{d,4}=ss/sum(data{d,3}(:));
g=index*100/tot;
an1=num2str(g);
middle1='%';
Progress=[an1,middle1]
index=index+1;

end
```

This block calculates the Pearson's coefficient as defined by equation 1, clears computer memory from temporary variables and stores output data:

```
display('Starting calculation of Pearson Coefficient')
for v=1:2:sis
k=size(data{v,3});
k=k(1,1)*k(1,2);
ss=0;
aa=0;
bb=0;
cc=0;
d=v+1;
vavg=mean(data{v,3}(:));
davg=mean(data{d,3}(:));


        for i=1:k
    s=(data{v,3}(i)-vavg)*(data{d,3}(i)-davg);
    ss=ss+s;

    a=((data{v,3}(i)-vavg)^2);
```

```
    aa=aa+a;
    b=((data{d,3}(i)-davg)^2);
    bb=bb+b;
        end
        cc=aa*bb;
    data{v,6}=ss/sqrt(cc);
    data{d,6}=data{v,6};
g=index*100/tot;
an1=num2str(g);
middle1='%';
Progress=[an1,middle1]
index=index+1;

end

clearvars -except data
display('results stored in data variable')
display('column 1: file name')
display('column 4: M1 and M2 coefficients')
display('column 5: overlap (Mander s) coefficient')
display('column 6: Pearson coeffiecient')
```

2D LIVE CELL IMAGING VIDEOS

SM1. Live cell 2D imaging video (51.4 sec) of PIP2 (green channel) and ACTIN (red channel) distributions, showing the interaction between these two bio-molecules during the cell adhesion process (10 minutes after cell seeding - 0.7 frames per second - time compression factor: 4.3). Field of view 50 µm x 50 µm.

SM2. Live cell 2D imaging video (53.3 sec) of PIP2 (green channel) and ACTIN (red channel), showing the interaction between these two bio-molecules during the cell adhesion process (30 minutes after cell seeding - 0.15 frames per second - time compression factor: 26.7). Field of view 55 µm x 55 µm.

REFERENCES

1 Du, J. & Armes, S. P. pH-Responsive Vesicles Based on a Hydrolytically Self-Cross-Linkable Copolymer. *Journal of the American Chemical Society* **127**, 12800-12801, doi: 10.1021/ja054755n (2005).

2 Wang, L. *et al.* Encapsulation of Biomacromolecules within Polymersomes by Electroporation. *Angewandte Chemie International Edition* **51**, 11122-11125, doi:10.1002/ anie.201204169 (2012).

3 Ruysschaert, T. *et al.* Hybrid Nanocapsules: interactions of ABA Block Copolymers with Liposomes. *Journal of the American Chemical Society* **127**, 6242-6247, doi:10.1021/ ja043600x (2005).

4 Canton, I. *et al.* Fully synthetic polymer vesicles for intracellular delivery of antibodies in live cells. *FASEB J* **27**, 98-108, doi:fj.12-212183 [pii] 10.1096/fj.12-212183 (2013).

5 Wehland, J. r., Osborn, M. & Weber, K. Phalloidin-induced actin polymerization in the cytoplasm of cultured cells interferes with cell locomotion and growth. *Proceedings of the National Academy of Sciences* **74**, 5613-5617 (1977).

6 To, C., Shilton, B. H. & Di Guglielmo, G. M. Synthetic Triterpenoids Target the Arp2/3 Complex and Inhibit Branched Actin Polymerization. *J Biol Chem* **285**, 27944-27957, doi: 10.1074/jbc.M110.103036 (2010).

7 Van Meer, G. & de Kroon, A. I. P. M. Lipid map of the mammalian cell. *J Cell Sci* **124**, 5-8, doi:Doi 10.1242/Jcs.071233 (2011).

8 Van den Bogaart, G. *et al.* Membrane protein sequestering by ionic protein-lipid interactions. *Nature* **479**, 552-555, doi:http://www.nature.com/nature/journal/v479/n7374/ abs/nature10545.html#supplementary-information (2011).

9 Botelho, R. J. *et al.* Localized biphasic changes in phosphatidylinositol-4,5-bisphosphate at sites of phagocytosis. *J Cell Biol* **151**, 1353-1368 (2000).

10 McLaughlin, S., Wang, J., Gambhir, A. & Murray, D. PIP2 AND PROTEINS: Interactions, Organization, and Information Flow. *Annual Review of Biophysics and Biomolecular Structure* **31**, 151-175, doi:doi:10.1146/annurev.biophys.31.082901.134259 (2002).

11 Virtanen, J. A., Cheng, K. H. & Somerharju, P. Phospholipid composition of the mammalian red cell membrane can be rationalized by a superlattice model. *Proceedings of the National Academy of Sciences* **95**, 4964-4969 (1998).

12 Simons, K. & Van Meer, G. Lipid sorting in epithelial cells. *Biochemistry* **27**, 6197-6202, doi:10.1021/bi00417a001 (1988).

13 Manders, E. M. M., Verbeek, F. J. & Aten, J. A. Measurement of co-localization of objects in dual-colour confocal images. *Journal of Microscopy* **169**, 375-382, doi:10.1111/j. 1365-2818.1993.tb03313.x (1993).

14 Dietrich, C. *et al.* Lipid Rafts Reconstituted in Model Membranes. *Biophysical Journal* **80**, 1417-1428, doi:http://dx.doi.org/10.1016/S0006-3495(01)76114-0 (2001).